Large scale zig-zag pattern emerging from circulating active shakers

Gaspard Junot,[1] Marco De Corato,[2] and Pietro Tierno[1,3,4,*]

[1] *Departament de Física de la Matèria Condensada, Universitat de Barcelona, 08028 Spain*
[2] *Aragon Institute of Engineering Research (I3A), University of Zaragoza, Zaragoza, Spain*
[3] *Universitat de Barcelona Institute of Complex Systems (UBICS), Universitat de Barcelona, Barcelona, Spain*
[4] *Institut de Nanociència i Nanotecnologia, Universitat de Barcelona, Barcelona, Spain*

(Dated: June 7, 2023)

We report the emergence of large zig-zag bands in a population of reversibly actuated magnetic rotors that behave as active shakers, namely squirmers that shake the fluid around them without moving. The shakers collectively organize into dynamic structures displaying self-similar growth, and generate topological defects in form of cusps that connect vortices of rolling particles with alternating chirality. By combining experimental analysis with particle-based simulation, we show that the special flow field created by the shakers is the only ingredient needed to reproduce the observed spatiotemporal pattern. We unveil a self-organization scenario in a collection of driven particles in an elastic medium emerging from the reduced particle degrees of freedom, as here the frozen orientational motion of the shakers.

Viscoelasticity, namely the tendency of a material to display both viscous and elastic response under external deformation, is commonly observed in a broad range of systems, from anelastic solids [1, 2], to liquid crystals [3], micelles [4], concentrated colloidal suspensions [5, 6] biopolymers [7, 8] or living cells [9, 10]. In viscoelastic fluids, the internal molecular rearrangement span several time and length scales, provoking a series of intriguing phenomena including stress relaxation, hysteresis, memory, creep or shear thickening [11]. While the bulk behavior of such fluids has been the matter of much research to date, emergent directions point towards investigating how such fluids mediate the organization of dispersed microscopic particles. Active [12–16], passive [17–19] or externally driven [20–25] particles in viscoelastic fluids are excellent model systems for many-body organization in elastic materials, while displaying promising applications in microrheology [26, 27], tissue engineering [28–30] or microrobotics [31, 32]. Indeed fluid elasticity can directly affect the propulsion behavior of microswimmers [33–40], or even be used to obtain net motion via streaming flow when pair of particles interact [36, 41, 42]. However, most of these works have been focused on single or few interacting particles, leaving the rich physics of ensembles a rich ground for exploration.

Here we demonstrate that a collection of active shakers made of driven magnetic microrotors can self organize into large scale dynamic bands displaying a zig-zag shape. First, we experimentally determine the flow field around a microrotor which originates from a microscopic version of the Weissenberg effect [44–46], and is astonishingly similar to that of a shaker force dipole [47]. Finite element simulations confirm that the elastic stresses around the periodically rotating particles drive a net dipolar flow field. We then characterize the growth process which starts at a microscopic level with pairs of rotors and grows beyond the millimeter scale. We found that the growth is scale invariant and linear with time. Using particle-based simulations based on a minimal model, we show that the shaker-like flow is at the origin of the instability, and it explains the observed constant angle of the bands. These results suggest that the formation of zig-zag patterns is a general effect which could arise in a broad range of systems.

We disperse anisotropic microparticles in a solution of polyacrylamide (PAAM) at a concentration of 0.05% by vol. in deionized water, (see Supplemental Material (SM) for more details [43]. The PAAM is a linear, high-molecular weight polymer ($M_w = 5 - 6 \cdot 10^6$) and its addition to water made the solution viscoelastic, see SM [43] for further details. From previous works [48, 49] we estimate the stress relaxation time of such diluted PAAM solution to be of the order $\tau \sim 3$ms. Within our PAAM solution we then disperse home-made ferromagnetic hematite colloids, prepared using a sol-gel technique [43, 50] and characterized by a peanut-like shape with two lobes with a long (short) axis equal to $\alpha = 2.6\,\mu$m ($\beta = 1.2\,\mu$m), see inset in Fig. 1a. The particles display a permanent magnetic moment of amplitude $m \simeq 9 \cdot 10^{-16}\,\mathrm{Am}^2$ [51], and oriented perpendicular to their long axis. Once dispersed in the PAAM solution, the particles sediment due to density mismatch, and float at an almost fixed elevation h due to the balance between gravity and electrostatic repulsion with the close substrate.

We realize active colloidal shakers by cyclically driving our particles back and forward along a fixed direction (here the $\hat{\boldsymbol{x}}$-axis) using a time dependent rotating field,

$$\boldsymbol{B} = B\left[\sin\left(2\pi t \Delta f_-\right)\hat{\boldsymbol{x}} + \cos\left(2\pi t \Delta f_+\right)\hat{\boldsymbol{z}}\right] \quad , \qquad (1)$$

being $\Delta f_\pm = f \pm \delta f/2$ and δf the frequency difference between the two field components along the $\hat{\boldsymbol{x}}$ and $\hat{\boldsymbol{z}}$ axis. The applied modulation periodically changes the direc-

* ptierno@ub.edu

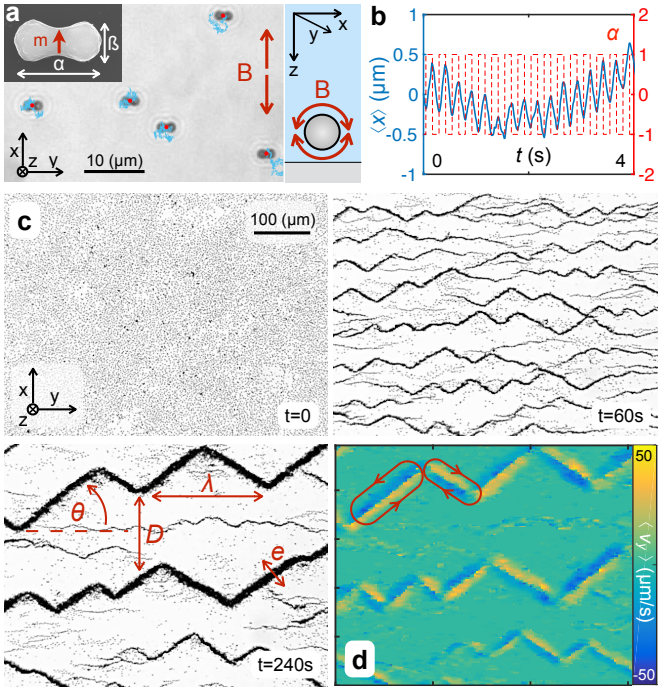

FIG. 1. (a) Trajectories of a dilute suspension of shakers after $N = 68$ cycles of the rotating field, MovieS1 in [43]. Top inset shows scanning electron microscope image of one hematite particle with the permanent magnetic moment $\boldsymbol{m}$. Small scheme on the right side shows lateral view of one magnetic roller. (d) Mean displacement $\langle x \rangle$ versus time t of shakers (blue) after $N = 16$ field cycles. Red line denotes the field direction of rotation α. (c) Sequence of images illustrating the band formation from an initially disordered suspension ($t = 0$) and under a magnetic modulation with $f = 80$Hz and $\delta t = 1/8$s, see also MovieS3 in [43]. The image at $t = 240$ s shows two bands at a distance D with wavelength λ, bond angle θ and thickness e. (d) Average horizontal velocity $\langle v_y \rangle$ of the shakers in bands. Red arrows denote the direction of the circulating particles, MovieS4 in [43].

tion of rotation α every $\delta t = 1/(2\delta f)$, inducing a magnetic torque $\boldsymbol{\tau}_m = \boldsymbol{m} \times \boldsymbol{B}$ that sets the particles into rotational motion around their short axis with an angular speed $\Omega = 2\pi f$ for frequencies $f < 100$Hz (synchronous regime). Moreover, since the applied field is circularly polarized along the $(\hat{\boldsymbol{x}}, \hat{\boldsymbol{z}})$ plane, it aligns the permanent moments of the particles, ensuring a fixed angular orientation. Here we fix $B = 5.5$mT and $f = 80$Hz.

The presence of a solid surface breaks the spatial symmetry, and produces a rolling transport due to the rotation-translation hydrodynamic coupling [52]. In the limit $\delta f = 0$, the field does not switches, and the hematite particles roll above the substrate by acquiring a frequency tunable propulsion speed $v_x \sim 2\pi\beta f$ [53], with β the particle short axis. In contrast, for a finite frequency delay $\delta f = 4$Hz, individual particles perform small oscillations of amplitude $\Delta x \sim 0.5\mu$m and zero average velocity, Fig. 1b and MovieS1 in [43].

The small amplitude time-reversible motion of the particle should produce no net displacement in a Newtonian fluid [54], as shown in MovieS2 in [43]. Instead, we find that, at high particle density $\phi = 0.117 \pm 0.002$, the shakers organize in complex dynamic bands which grow linearly with time. As shown in the sequence of images in Fig. 1c, a system of randomly distributed particles evolves into a structured array of bands with zig-zag like shape after few second of magnetic driving. The bands grow first by acquiring nearest particles, located on their lateral sides, and then via a continuous merging, MovieS3 in [43]. These dynamic bands acquire a zig-zag shape with branches arranged at a constant angle of $\theta_l = \pm 31°$ delimited by cusps. A careful inspection of the particle velocity within a band, Fig. 1d, reveals that the shakers move collectively forming rotating vortices with fast circulating edge currents up to $50\mu\text{m}\,\text{s}^{-1}$, MovieS3 in [43]. Each branch of a band is made of a large scale vortical flow of particles, and cusps within a band connects vortices of opposite chirality, similar to a two gears system. These bands were observed to form also for smaller peanuts ($\alpha = 1.8\,\mu$m, $\beta = 1.3\,\mu$m), or by varying $f \in [40, 100]$Hz and for $\delta f > 0.75$Hz.

To understand these unexpected, complex structures we analysed the flow field generated by a single microrotor. We obtain the velocity field in a dilute suspension of microrotor over many field periods via particle tracking velocimetrysee SM for details [43]. Note that in a Newtonian fluid hydrodynamics interactions are time reversible so that no net particle displacement would emerge. Strikingly, the obtained flow field in Fig. 2(a), displays strong similarities with that generated by a shaker-like force dipole [47]. Shakers are a category of squimers that generate a flow pattern similar to that of several microorganisms such as *Escherichia coli* bacteria [55] but without the polar component, which prevent them from self-propelling. These particles exert stresses on the surrounding fluid [56–58] that drive a flow field displaying an attracting part at the particle sides and a repulsive one at the tips, with a recirculation vortex between these two regions. An estimate of the Deborah number, $De = 2\pi f \tau$, yields $De \approx 1.5$, which suggests that this particular flow field results from the fluid elasticity. Thus, the particle rotation induces a normal stress difference along the $\hat{\boldsymbol{x}}$-axis which induces a flow toward the rotor and, by volume conservation, the fluid is expelled toward the tips, Fig. 2(b). We confirm this hypothesis by computing the flow velocity $\mathbf{v}$ around a periodically-rotating ellipsoid via three-dimensional numerical simulations. We consider a stress tensor $\mathbf{T} = -p\mathbf{I} + \eta_s \left(\nabla\mathbf{v} + \nabla\mathbf{v}^T\right) + \sigma$ as sum of a Newtonian contribution (viscosity of water η_s) coming from the solvent and a viscoelastic one σ introduced by the PAAM. Here p is the pressure that enforce the incompressibility condition, $\nabla \cdot \mathbf{T} = \mathbf{0}$. We use the Oldroyd-B constitutive model, which predicts a constant

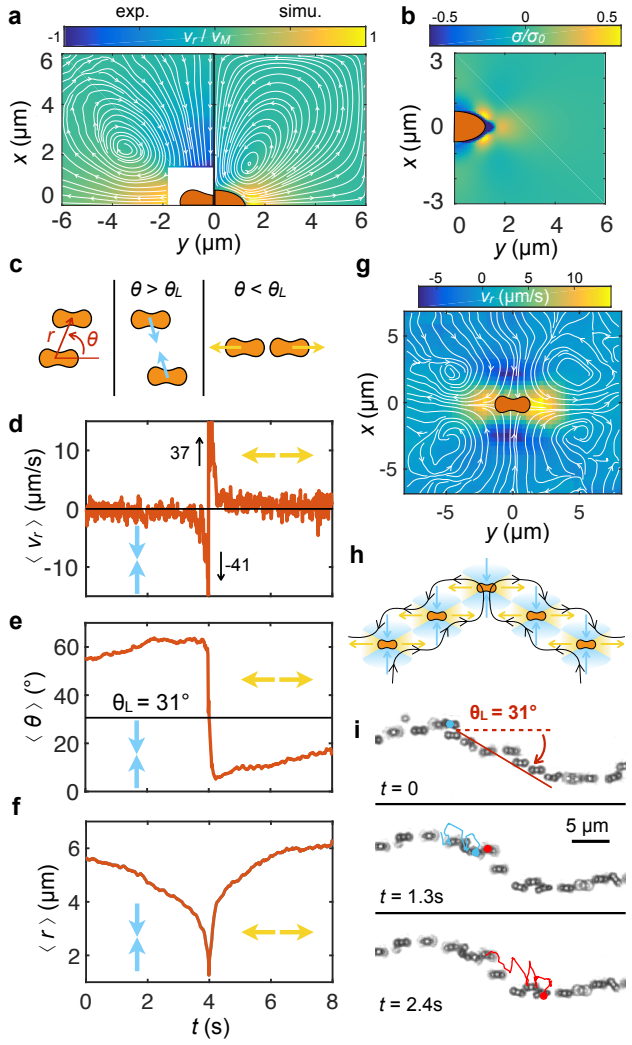

FIG. 2. (a) Normalized relative velocity v_r/v_M in the (x, y) plane of one shaker showing regions of attractions ($v_r < 0$) and repulsion ($v_r > 0$) separated by θ_l. Left (right) panel refers to experimentally measured (simulated) flow field velocity normalized by the maximum velocity v_M with superimposed the flow streamlines ($v_M = 2.2\,\mu\mathrm{m\,s}^{-1}$ for the experiments, $v_M = 22\mu\mathrm{m\,s}^{-1}$ for the simulation see also the SM [43]). (b) Normalized first normal stress difference in the (x, y) plane with $\sigma_0 = (\eta_s + \eta_p)\omega$, see text. (c) Schematics of two microrotors in three configurations: attraction (repulsion) arises when $\theta > \theta_l$ ($\theta < \theta_l$) with $\theta_l = 31°$. (d-f) Evolution with time of (d) the average radial velocity $\langle v_r \rangle$, (e) the relative angle $\langle \theta \rangle$ and (f) the radial distance $\langle r \rangle$ between two approaching microrotors. In all images blue (yellow) arrows indicate attraction (repulsion) between the pair, MovieS5 in [43]. (g) Top view of the flow velocity generated from the interaction of two shakers. (h) Assembled structure from the flow produced by the shakers. (i) Sequence of snapshots showing a one-particle thin band with superimposed two particle's trajectories, MovieS6 in [43].

viscosity but a non zero normal stress difference [59], via an additional constitutive equation:

$$\tau\left(\frac{\partial}{\partial t}\sigma + \mathbf{v}\cdot\nabla\sigma - \nabla\mathbf{v}\cdot\sigma - \sigma\cdot\nabla\mathbf{v}^T\right) + \sigma = \eta_p\left(\nabla\mathbf{v} + \nabla\mathbf{v}^T\right) \ , \tag{2}$$

where η_p is the polymer viscosity. Such model reduces to only two parameters, η_p and $\tau \sim 3$ ms. The polymer viscosity can be extracted from the zero-shear viscosity of the solution, which from the experimental measurements is $\eta_0 \approx 2\ \eta_s$ thus we estimate $\eta_p \approx \eta_s$. See SM [43] for further technical details.

The right panel of Fig. 2(a) shows that the computed velocity field in the plane $z = h$ and averaged over one period, δt, displays the same features as that measured in the experiments and confirms that the mechanism driving the dipolar flow structure is the first normal stress difference, see Fig. 2(b). This result is consistent with the seminal works by Giesekus [60] and Fosdick and Kao [61], who showed that the first normal stress distribution around a rotating sphere generates streamlines that increase with even powers of De. It follows that the flow field introduced by the first normal stresses does not change sign upon changing the direction of the particle rotation leading to a non zero average over one period.

We then analysed the interactions between a pair of shakers using data from 33 separate experiments. Due to the field alignment, the magnetic particles display neg-

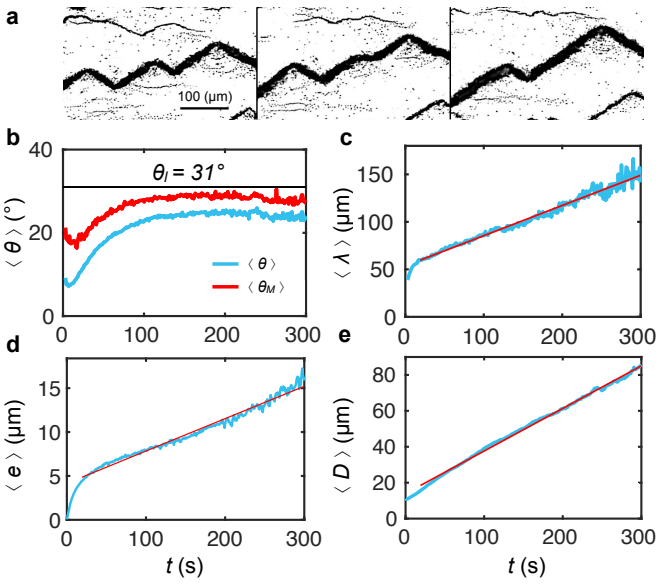

FIG. 3. (a) Sequence of snapshots showing the annihilation of a cusp (total duration $\Delta t = 30$ s), MovieS7 in [43]. Coarsening dynamics: time evolution of the mean angle $\langle\theta\rangle$ (b), wavelength $\langle\lambda\rangle$ (c), thickness $\langle e\rangle$ (d) and distance $\langle D\rangle$ (e). After a short transitory, λ, e and D all scale linearly with time (red line) while θ set to a stationary value of $\theta_l = 31°$. In (b) $\langle\theta\rangle$ corresponds to the full average over the experimental data, weighted by the size of the zig-zag bands, while $\langle\theta_M\rangle$ is its maximal value over the bands.

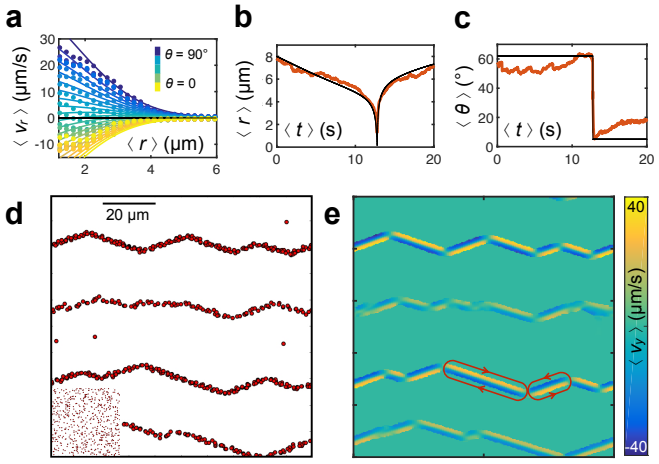

FIG. 4. (a) Average radial velocity $\langle v_r \rangle$ between two particles as function of their relative distance r and for different angle θ (colorbar). Scattered data are experiments while continuous line are non-linear regression using Eq. 9 in [43]. (b,c) Average radial distance (b) and relative angle (c) as function of time for pairs of interacting particles. In both graphs, experiments (simulation) are represented by the red (black) curve. (d) Image showing the zig-zag state obtained after a time $t = 50$ s with $N = 601$ particles, MovieS8 in [43]. Small inset shows the initial random configuration of the particles. (e) Corresponding color-coded plot showing the average translational velocity $\langle v_y \rangle$ with two red arrows denoting the direction of the circulating rotors.

ligible orientational motion and the relative orientation can be described in term of a single angle θ, Fig. 2c. The relative velocity field between the pair has a similar structure than the one generated by a single one. Two particles attract each other when are side by side and repel when positioned tip-to-tip. The transition between the two regions occurs at an angle $\theta_l = 31°$, Fig. 2(c). When two particles are initially arranged such that $\theta > \theta_l$, they approach first slowly and keeping their relative orientation constant. Near close contact, $r = 2\mu$m we observe a rapid sliding process which causes a speed up effect reaching relative velocities up to $v_r = 40\mu\text{ms}^{-1}$, Fig. 2(d-f). Such process re-arrange the rotors from side-by side ($\theta \sim 60°$) to tip-to-tip ($\theta \sim 0°$), MovieS5 in [43]. Thus, close particles arrange themselves at an angle θ_l where attraction and repulsion are minimized and, by drawing the flow lines, one recovers the direction of rotation of the vortices, Fig. 2h. During band growth, defects arises in form of cusps which sink incoming particles expelling them from the opposite side, Fig. 2g. Such hypothesis is confirmed by observing the formation of one line thin band, Fig. 2i and MovieS6 in [43], where the constituent particles detaching from the branch are dragged along the vortical edge current toward the nearest cusp.

Ensemble of shakers exhibit a self-similar behaviour with scale invariance in time as they evolve to large scale structures, Fig. 3a. During coarsening, the different band parameters as wavelength (λ, Fig. 3c), thickness (e, Fig. 3d) and distance (D, Fig. 3e) grow linearly in time, while the the bond angle rapidly saturate to θ_l, Fig. 3b [62]. As shown in Fig.3a, a band is composed of a sequence of topological defects in form of positive (pointing upwards) and negative cusps that connect different branches in a zig-zag manner. During coarsening, small branches disappear in favor of large one inducing the annihilation of cusps, MovieS7 in [43]. This dynamically slow process ultimately would lead to a single band of particles, or to separate bands at very large distance between them. However, due to the slow velocity of coarsening and the large system size (observation window 0.66 mm, whole system size 1 cm), this state is difficult to reach experimentally. During coarsening, separate bands merge by reducing their distance until touching each other. Such process is triggered in part by the cusp annihilation that increases the wavelength λ and so the spatial extension of a band along the lateral direction ($\hat{\boldsymbol{x}}$). The fusion of two bands increases the inter-band distance D and give rise to a new structure with larger thickness e. This new band will in turn annihilates its cusps, starting a new cycle. The cusp's annihilation process ($[A] + [A] \to 0$) can be written as $\frac{d[A]}{dt} = -k[A]^2$, being $[A]$ the linear cusp concentration and k the annihilation rate. The solution of this equation is $[A](t) = a_0/(1 + a_0 kt)$ with $a_0 = [A](t = 0)$. Thus, one can recover the linear growth in time of the wavelength by writing, $\lambda(t) = 2/[A] = 2(kt + 1/a_0)$.

To rationalize our results, we set-up a minimal simulation scheme that reproduces the self-organization scenario neglecting magnetic and steric interactions. The former are not considered given the relative low value of $\boldsymbol{m}$. For two hematite rotors (i, j) aligned tip to tip (side by side) at the closest distance of $x_{ij} = \beta$ ($y_{ij} = \alpha$) the time averaged potential is relatively weak, given by $\langle U_d \rangle = -\mu_0 m^2/(8\pi x_{ij}^3) = -5.8\, k_B T$ ($\langle U_d \rangle = \mu_0 m^2/(4\pi x_{ij}^3) = 1.1\, k_B T$ resp.), being $\mu_0 = 4\pi 10^{-7}\,\text{Hm}^{-1}$. Thus, we are left to consider the generated velocity field (see Fig. 4a) that we obtain directly from the experimental data. We use an empirical function which simultaneously fit all data (Eq. 9 in SM [43]) and provides the relative velocity $\boldsymbol{v}(r_{ij}; \theta_{ij})$ between particles at relative position r_{ij} and orientation θ_{ij}. Thus, we numerically integrate the equation of motion $\frac{d\boldsymbol{r}_i}{dt} = \sum_{i \neq j} \boldsymbol{v}(r_{ij}; \theta_{ij})$, more details on the implementation can be found in the SM [43]. Taking into account the different approximation used, the result is rather striking since it allow to reproduced the band formation process and predict the correct circulation flow across the bands, as shown in Fig. 4(d,e). Thus, the zigzag pattern arise due to the shaker-like shape of the flow field generated by the particle rotation, MovieS8 in [43].

In conclusion, we show that zig-zag bands emerge be-

cause of the shaker-like flow field generated by the magnetic rotors. In our system, this flow field results from the elastic stress created by the particle rotation within the PAAM solution. However, similar patterns have been also reported in Newtonian fluids for particles submitted to an AC field [63]. The physical origin of this instability was explain by macroscopic gradients in the electrolyte concentration due to the field-induced concentration gradients near the particles surfaces [64, 65]. Further, such instability was attributed to mutual polarization of particles, causing them to rotate [66, 67], and recently to the presence of electrokinetic flows [68]. Our work shows that the zigzag instability is even more general, suggesting that it is not the the forcing (magnetic or electric) nor the medium (Newtonian or viscoelastic) that matter but rather the type of hydrodynamic flow those systems create around the particle. The frozen orientation of the shakers plays an important role in stabilizing the zigzags. Indeed, in active nematics it was shown that freezing one orientation via a constant magnetic field induces a zig-zag stripe phase [69]. In contrast, systems of force-dipoles free to rotate and/or able to self propelled may not exhibit such stable structures as they generate turbulent dynamics. Thus, we find that the zigzag instability is a general phenomenon that would depend only on the symmetry of the flow field developed by the particles. A potential technological application of our work could be to localize magnetic inclusions in a microfluidc device. The oscillating field could be used for example to control the flow by inducing (removing) clogging when oscillating field is switched on (off).

We thank Thomas M. Fischer and Jaume Casademunt for stimulating discussions, and Jordi Ortín for help with the rheological measurements. This work has received funding from the European Research Council (ERC Consolidator Grant contract No. 811234). P. T. acknowledge support from the program "ICREA Acadèmia". M.D.C. acknowledges funding the Spanish Ministry of Science and Innovation (MCINN) under the Juan de la Cierva (IJC2018-035270-I) postdoctoral fellowship and the retos de investigación grant PID2020-113033GB-I00.

[1] A. C. Pipkin, Small finite deformations of viscoelastic solids, Rev. Mod. Phys. **36**, 1034 (1964).
[2] T. Jaglinski, D. Kochmann, D. Stone, and R. S. Lakes, Composite materials with viscoelastic stiffness greater than diamond, Science **315**, 620 (2007).
[3] P. G. de Gennes and J. Prost, The Physics of Liquid Crystals (Oxford University Press, London, UK, 2001).
[4] D. T. Chen, Q. Wen, P. A. Janmey, J. C. Crocker, and A. G. Yodh, Rheology of soft materials, Annu. Rev. Condens. Matter Phys. **1**, 301 (2010).
[5] T. G. Mason and D. A. Weitz, Linear viscoelasticity of colloidal hard sphere suspensions near the glass transition, Phys. Rev. Lett. **75**, 2770 (1995).
[6] G. L. Hunter and E. R. Weeks, The physics of the colloidal glass transition, Rep. Prog. Phys. **75**, 066501 (2012).
[7] C. Storm, J. J. Pastore, F. C. MacKintosh, T. C. Lubensky, and P. Janmey, Nonlinear elasticity in biological gels, Nature **435**, 191–194 (2005).
[8] G. H. Koenderink, D. Zvonimir, N. Fumihiko, P. M. Bendix, F. C. Mackintosh, J. H. Hartwig, T. P. Stossel, and D. A. Weitz, An active biopolymer network controlled by molecular motors, Proc. Natl. Acad. Sci. U.S.A. **106**, 15192–15197 (2009).
[9] X. Trepat, L. Deng, S. S. An, D. Navajas, D. J. Tschumperlin, W. T. Gerthoffer, J. P. Butler, and J. J. Fredberg, Universal physical responses to stretch in the living cell, Nature **447**, 592–595 (2007).
[10] J.-T. Hang, G.-K. Xu, and H. Gao, Frequency-dependent transition in power-law rheological behavior of living cells, Science Advances **8**, 4001 (2022).
[11] P. Oswald, Rheophysics: The Deformation and Flow of Matter (Cambridge University Press, London, UK, 2014).
[12] J. R. Gomez-Solano, A. Blokhuis, and C. Bechinger, Dynamics of self-propelled janus particles in viscoelastic fluids, Phys. Rev. Lett. **116**, 138301 (2016).
[13] G. Li and A. M. Ardekani, Collective motion of microorganisms in a viscoelastic fluid, Phys. Rev. Lett. **117**, 118001 (2016).
[14] C. kuan Tung, C. Lin, B. Harvey, A. G. Fiore, F. Ardon, M. Wu, and S. S. Suarez, Fluid viscoelasticity promotes collective swimming of sperm, Sci. Reports **7**, 3152 (2017).
[15] C. Lozano, J. R. Gomez-Solano, and C. Bechinger, Active particles sense micromechanical properties of glasses, Nat. Materials **18**, 1118–1123 (2019).
[16] G. Li, E. Lauga, and A. M. Ardekan, Microswimming in viscoelastic fluids, J. Non New. Mech. **297**, 104655 (2017).
[17] I. I. Smalyukh, O. D. Lavrentovich, A. N. Kuzmin, A. V. Kachynski, and P. N. Prasad, Elasticity-mediated self-organization and colloidal interactions of solid spheres with tangential anchoring in a nematic liquid crystal, Phys. Rev. Lett. **95**, 157801 (2005).
[18] J. Kotar, M. Vilfan, N. Osterman, D. c. v. Babič, M. Čopič, and I. Poberaj, Interparticle potential and drag coefficient in nematic colloids, Phys. Rev. Lett. **96**, 207801 (2006).
[19] S. Park, Q. Liu, and I. I. Smalyukh, Colloidal surfaces with boundaries, apex boojums, and nested elastic self-assembly of nematic colloids, Phys. Rev. Lett. **117**, 277801 (2016).
[20] S. Hernàndez-Navarro, P. Tierno, J. A. Farrera, J. Ignés-Mullol, and F. Sagués, Reconfigurable swarms of nematic colloids controlled by photoactivated surface patterns, Angew. Chem. Int. Ed. **53**, 10696 (2014).
[21] G. D'Avino and P. L. Maffettone, Particle dynamics in viscoelastic liquids, J. Non Newtonian Fluid Mech. **215**, 80 (2015).
[22] J. Puente-Velázquez, F. A. Godínez, E. Lauga, and R. Zenit, Viscoelastic propulsion of a rotating dumbbell, Microfluidics and Nanofluidics **23**, 1 (2019).
[23] G. Junot, X. Wei, J. Ortín, R. Golestanian, Y. Wang, P. Tierno, and F. Meng, Elastically-mediated collective organisation of magnetic microparticles., Soft Matter **18**, 5171 (2022).

[24] L. W. Rogowski, J. Ali, X. Zhang, J. N. Wilking, H. C. Fu, and M. J. Kim, Symmetry breaking propulsion of magnetic microspheres in nonlinearly viscoelastic fluids., Nat. Comm. **12**, 1116 (2021).

[25] Y. Su, A. Castillo, O. Shun Pak, L. Zhu, and R. Zenit, Viscoelastic levitation, J. Fluid Mech. **943**, A23 (2022).

[26] D. Winter, J. Horbach, P. Virnau, and K. Binder, Active nonlinear microrheology in a glass-forming yukawa fluid, Phys. Rev. Lett. **108**, 028303 (2012).

[27] M. Khan, K. Regan, and R. M. Robertson-Anderson, Optical tweezers microrheology maps the dynamics of strain-induced local inhomogeneities in entangled polymers, Phys. Rev. Lett. **123**, 038001 (2019).

[28] K. Y. Lee and D. J. Mooney, Hydrogels for tissue engineering., Chem. Rev. **101**, 1869–1880 (2001).

[29] B. J. Kwee and D. J. Mooney, Biomaterials for skeletal muscle tissue engineering, Current Opinion in Biotechnology **47**, 16 (2017).

[30] M. Cianchetti, C. Laschi, A. Menciassi, and P. Dario, Biomedical applications of soft robotics., Nat. Rev. Mater. **3**, 143–153 (2018).

[31] S. Fusco, M. S. Sakar, S. Kennedy, C. Peters, R. Bottani, F. Starsich, A. Mao, G. A. Sotiriou, S. Pané, S. E. Pratsinis, D. Mooney, and B. J. Nelson, An integrated microrobotic platform for on-demand, targeted therapeutic interventions, Advanced Materials **26**, 952 (2014).

[32] S. Palagi and P. Fischer, Bioinspired microrobots, Nat. Rev. Mater. **3**, 113–124 (2018).

[33] H. C. Fu, T. R. Powers, and C. W. Wolgemuth, Theory of swimming filaments in viscoelastic media, Phys. Rev. Lett. **99**, 258101 (2007).

[34] J. Teran, L. Fauci, and M. Shelley, Viscoelastic fluid response can increase the speed and efficiency of a free swimmer, Phys. Rev. Lett. **104**, 038101 (2010).

[35] X. N. Shen and P. E. Arratia, Undulatory swimming in viscoelastic fluids, Phys. Rev. Lett. **106**, 208101 (2011).

[36] O. S. Pak, L. Zhu, L. Brandt, and E. Lauga, Micropropulsion and microrheology in complex fluids via symmetry breaking, Phys. Fluids **24**, 103102 (2012).

[37] S. E. Spagnolie, B. Liu, and T. R. Powers, Locomotion of helical bodies in viscoelastic fluids: Enhanced swimming at large helical amplitudes, Phys. Rev. Lett. **111**, 068101 (2013).

[38] B. Thomases and R. D. Guy, Mechanisms of elastic enhancement and hindrance for finite-length undulatory swimmers in viscoelastic fluids, Phys. Rev. Lett. **113**, 098102 (2014).

[39] J. P. Binagia and E. S. G. Shaqfeh, Self-propulsion of a freely suspended swimmer by a swirling tail in a viscoelastic fluid, Phys. Rev. Fluids **6**, 053301 (2021).

[40] P. E. Arratia, Life in complex fluids: Swimming in polymers, Phys. Rev. Fluids **7**, 110515 (2022).

[41] C. Datt, B. Nasouri, and G. J. Elfring, Two-sphere swimmers in viscoelastic fluids, Phys. Rev. Fluids **3**, 123301 (2018).

[42] L. A. Kroo, J. P. Binagia, N. Eckman, M. Prakash, and E. S. Shaqfeh, A freely suspended robotic swimmer propelled by viscoelastic normal stresses, Phys. Fluids **24**, 103102 (2022).

[43] See EPAPS Document No.xxxx which includes one file with details of the experiments and numerical simulation, eight supplementary videos and Refs [70–73].

[44] K. Weissenberg, A continuum theory of rhelogical phenomena, Nature **159**, 310–311 (1947).

[45] D. Janes and H. Thomas, Weissenberg effect as an end-point in coagulation studies., Nature **216**, 197–198 (1967).

[46] A. S. Lodge, J. D. Schieber, and R. B. Bird, The weissenberg effect at finite rod-rotation speeds, J. Chem. Phys. **88**, 4001 (1988).

[47] Y. Hatwalne, S. Ramaswamy, M. Rao, and R. A. Simha, Rheology of active-particle suspensions, Phys. Rev. Lett. **92**, 118101 (2004).

[48] A. Zell, S. Gier, S. Rafai, and C. Wagner, Is there a relation between the relaxation time measured in caber experiments and the first normal stress coefficient?, J. Non-Newton. Fluid. Mech. **165**, 1265 (2010).

[49] F. Del Giudice, G. D'Avino, F. Greco, I. De Santo, P. A. Netti, and P. L. Maffettone, Rheometry-on-a-chip: measuring the relaxation time of a viscoelastic liquid through particle migration in microchannel flows, Lab on a Chip **15**, 783 (2015).

[50] T. Sugimoto, M. M. Khan, and A. Muramatsu, Preparation of monodisperse peanut-type α-fe$_2$o$_3$ particles from condensed ferric hydroxide gel, Colloids Surf. A **70**, 167 (1993).

[51] F. Martinez-Pedrero, E. Navarro-Argemí, A. Ortiz-Ambriz, I. Pagonabarraga, and P. Tierno, Emergent hydrodynamic bound states between magnetically powered micropropellers, Sci. Adv. **4**, aap9379 (2018).

[52] J. Happel and H. Brenner, Low Reynolds Number Hydrodynamics (Noordhoff, Leyden, The Netherlands, 1973).

[53] G. Junot, A. Cebers, and P. Tierno, Collective hydrodynamic transport of magnetic microrollers., Soft Matter **17**, 8605 (2021).

[54] E. M. Purcell, Life at low reynolds number, Am. J. Phys. **45**, 3 (1977).

[55] E. Lauga and T. R. Powers, The hydrodynamics of swimming microorganisms, Rep. Prog. Phys. **72**, 096601 (2009).

[56] Y. Hatwalne, S. Ramaswamy, M. Rao, and R. A. Simha, Rheology of active-particle suspensions, Phys. Rev. Lett. **92**, 118101 (2004).

[57] K. V. S. Chaithanya and S. P. Thampi, Deformation dynamics of an active compound particle in an imposed shear flow-a theoretical study, J. Phys. D: Appl. Phys. **53**, 314001 (2020).

[58] A. Scagliarini and I. Pagonabarraga, Hydrodynamic and geometric effects in the sedimentation of model run-and-tumble microswimmers, Soft Matter **18**, 2407 (2022).

[59] R. G. Larson, Constitutive equations for polymer melts and solutions (Butterworth-Heinemann, 2013).

[60] H. Giesekus, Proceedings of the Fourth International Congress on Rh (1965).

[61] R. L. Fosdick and B. G. Kao, Steady flow of a simple fluid around a rotating sphere, Rheol. Acta **19**, 675 (1980).

[62] To avoid that the averaged values are dominated by the small structures that are more numerous than the large ones but only contain a small fraction of the particles, $\langle\theta\rangle$, $\langle\lambda\rangle$ and $\langle e\rangle$ are weighted by the area of the zig-zag band. Thus, small zig-zag bands count less than larger ones.

[63] B. R. Jennings and M. Stankiewicz, Electro-optic observations of electrodynamic band formation in colloidal suspensions, Proc. R. Soc. Lond. A **427**, 321 (1990).

[64] H. Isambert, A. Ajdari, J.-L. Viovy, and J. Prost, Electrohydrodynamic patterns in charged colloidal solutions,

Phys. Rev. Lett. **78**, 971 (1997).
[65] H. Isambert, A. Ajdari, J.-L. Viovy, and J. Prost, Electrohydrodynamic patterns in macroion dispersions under a strong electric field, Phys. Rev. E **56**, 5688 (1997).
[66] Y. Hu, J. L. Glass, A. E. Griffith, and S. Fraden, Observation and simulation of electrohydrodynamic instabilities in aqueous colloidal suspensions, J. Chem. Phys. **100**, 4674 (1994).
[67] P. P. Lele, M. Mittal, and E. M. Furst, Anomalous particle rotation and resulting microstructure of colloids in ac electric fields, Langmuir **24**, 12842 (2008).
[68] F. Katzmeier, B. Altaner, J. List, U. Gerland, and F. C. Simmel, Emergence of colloidal patterns in ac electric fields, Phys. Rev. Lett. **128**, 058002 (2022).
[69] P. Guillamat, J. Ignés-Mullol, and F. Sagués, Control of active liquid crystals with a magnetic field, Proc. Nat. acad. Sci. USA **113**, 5498 (2016).
[70] W.-M. Kulicke, R. Kniewske, and J. Klein, Preparation, characterization, solution properties and rheological behaviour of polyacrylamide, Progr. pol. sci. **8**, 373 (1982).
[71] A. N. Brooks and T. J. R. Hughes, Streamline upwind/petrov-galerkin formulations for convection dominated flows with particular emphasis on the incompressible navier-stokes equations, Comput. Methods Appl. Mech. Eng. **32**, 199 (1982).
[72] R. Keunings, On the high weissenberg number problem, J. Non-Newt. Fluid Mech. **20**, 209 (1986).
[73] H. Massana-Cid, E. Navarro-Argemí, D. Levis, I. Pagonabarraga, and P. Tierno, Leap-frog transport of magnetically driven anisotropic colloidal rotors, J. Chem. Phys. **150**, 164901 (2019).